In-situ/operando Techniques for Unraveling Mechanisms of Ionic Transport in Solid-State Lithium Indium Halide Electrolyte

Farzaneh Bahmani * , Collyn Rodmyre , Karen Ly , Paul Mack , Alevtina White Smirnova

Posted Date: 29 November 2023

doi: 10.20944/preprints202311.1860.v1

Keywords: Solid-state batteries; lithium halides; temperature; pressure; In-situ XRD and XPS

Article

In-Situ/Operando Techniques for Unraveling Mechanisms of Ionic Transport in Solid-State Lithium Indium Halide Electrolyte

Farzaneh Bahmani [1,*], Collin Rodmyre [1], Karen Ly [1], Paul Mack [3] and Alevtina White Smirnova [1,2,*]

[1] Materials Engineering and Science program, South Dakota Mines, South Dakota 57701, USA; Farzaneh.Bahmani@mines.sdsmt.edu; Collin.Rodmyre@mines.sdsmt.edu; Karen.Ly@mines.sdsmt.edu
[2] Department of Chemistry, Biology, and Health Sciences, South Dakota Mines, South Dakota 57701, USA
[3] Thermo Fisher Scientific, East Grinstead, West Sussex, RH19 1UB, UK; Paul.Mack@thermofisher.com
* Correspondence: Alevtina.Smirnova@sdsmt.edu

Abstract: In the past years, lithium-ion solid-state batteries demonstrated significant advancements regarding such properties as safety, long-term endurance, and energy density. The properties of these depend on solid-state electrolytes and especially ionic transport interfacial transport with cathode or anode materials. Solid-state electrolytes based on lithium halides offer new opportunities due to their unique features such as broad electrochemical stability window, high lithium-ion conductivity, and elasticity at close to melting point temperatures that help to improve lithium-ion transport at interfaces. A comparative study of lithium indium halide (Li_3InCl_6) electrolytes synthesized by a mechano-thermal method using different optimization parameters revealed a significant effect of ball-milling time, temperature, and pressure on lithium-ion transport. Based on the Electrochemical Impedance Spectroscopy (EIS) data in the temperature range of 25-100 °C, the optimized Li_3InCl_6 electrolyte phase demonstrates high ionic conductivity reaching 0.98 mS cm^{-1} at room temperature. However, at 70 °C, phase transformation was observed leading to significant changes in the activation energy for lithium-ion transport. In-situ X-ray diffraction and in-situ/operando X-ray photoelectron spectroscopy techniques confirmed the temperature-dependent behavior of Li_3InCl_6 synthesized. These observations provide critical information for practical applications of solid-state electrolytes and nanocomposites based on Li_3InCl_6 within the broad temperature range for lithium-ion solid-state batteries with improved morphology, chemical interactions, and structural integrity.

Keywords: solid-state batteries; lithium halides; temperature; pressure; in-situ XRD and XPS

1. Introduction

The increasing demand for clean energy storage systems and the swift growth of the electric vehicle industry highlighted the safety concerns associated with conventional liquid lithium-ion batteries. These batteries use flammable liquid electrolytes and are susceptible to thermal runaway [1,2]. In contrast, solid-state batteries (SSBs) with solid-state electrolytes (SSEs) captured significant attention for their inherent non-flammable nature and safety [3,4]. Additionally, SSEs enable the use of a lithium metal anode, greatly enhancing the energy density of a battery to meet the rising demand for high-performance energy storage systems [5,6]. However, further research is needed to address the challenges associated with their development and to ensure their widespread commercialization. An essential aspect in this pursuit is the identification of highly conductive solid-state electrolytes possessing both high lithium-ion conductivity and electrochemical stability that are crucial for safe and energy-dense SSBs [7]. Current research in SSEs predominantly focuses on sulfide-based and oxide-based SSEs. Sulfide SSEs typically display substantial ionic conductivity (10^{-3} to 10^{-4} S cm^{-1}) at room temperature, along with good thermal stability and a broad electrochemical stability window [8]. However, they are extremely sensitive to the atmosphere, reacting readily with water and oxygen to generate toxic H_2S gas [9]. Furthermore, direct contact between sulfur-based SSEs and cathode results in substantial interfacial resistance due to side reactions, which are exacerbated by sulfide

Preprints (www.preprints.org) | NOT PEER-REVIEWED | Posted: 29 November 2023 doi:10.20944/preprints202311.1860.v1

SSEs' decomposition at high voltages. Specifically, the oxidation of the sulfur-based Li_6PS_5Cl electrolyte at the interface with positive electrode active materials, such as $LiCoO_2$, $LiNi_{1/3}Co_{1/3}Mn_{1/3}O_2$, and $LiMn_2O_4$, leads to the formation of elemental sulfur, lithium polysulfides, P_2S_x($x \geq 5$), phosphates, and LiCl [10].

In contrast, oxide-based solid electrolytes are air-stable, but demonstrate high resistances at electrolyte-cathode interfaces [11–13]. Furthermore, the oxide-based SSE synthesis involves high-temperature sintering, which causes side reactions between the electrode and oxide SSEs in the case of co-sintering [11]. These unfavorable factors have hindered further developments in oxide SSEs. To address these challenges, researchers have made notable advancements in the development of halide-based SSEs. Lithium halide electrolytes hold great promise regarding their high ionic conductivity, thermal stability, and wide electrochemical stability window over 4.0 V [14,15]. Among these, Li_3InCl_6 electrolytes show good potential regarding high ionic conductivity and compatibility with high-voltage cathode materials, such as $LiCoO_2$ and $LiNi_{0.8}Co_{0.1}Mn_{0.1}O_2$ (NCM) [16]. It was reported that a reversible areal capacity of 12.16 mAh cm^{-2} at 0.1 mA for NMC811/Li_3InCl_6/$Li_{10}GeP_2S_{12}$/In at room temperature [17] with a specific capacity of 27 mAh g^{-1} at 0.1C for $LiCoO_2$–Li_3InCl_6/Li_3InCl_6/In cell [15].

One of the Li_3InCl_6 -based electrolyte limitations is its sensitivity to moisture [18] which triggers reactions leading to lower ionic conductivity. Besides moisture, the influence of operating temperature on ionic conductivity emerged as a critical factor for practical applications. However, there is an absence of detailed studies exploring the temperature effect on Li_3InCl_6 electrolytes. Our research reveals a remarkable enhancement in the ionic conductivity of Li_3InCl_6 at elevated temperatures, highlighting its potential as an SSE for advanced energy storage systems.

In this study, an efficient and flexible solid-state mechano-thermal method for the synthesis of glass-ceramic Li_3InCl_6, utilizing different ball-milling times and annealing temperatures is presented. Through a comprehensive investigation of the ionic conductivity of Li_3InCl_6 SSEs across a wide temperature range and morphology, a detailed understanding of their behavior was acquired. In-situ X-ray powder diffraction (XRD) was used to track phase changes in solid-state electrolytes (SSEs) at varying temperatures. Furthermore, X-ray Photoelectron Spectroscopy (XPS) was applied to monitor the chemical changes with temperature.

2. Materials and Methods

2.1. Synthesis of Li_3InCl_6 solid-state electrolyte

The Li_3InCl_6 inorganic precursors, specifically LiCl (99.98%, Aladdin), and $InCl_3$ (99.99%, Aladdin) with a stoichiometric ratio of 3:1 were mixed and ground using agate mortar and pestle, and then mechanically mixed for 12 or 24 hours using a high-energy ball-mill at speed 600 rpm (Table 1). The ball-milled precursors were placed in a Schlenk tube inside the argon glovebox to prevent moisture absorption. Then the sealed tube is placed in the tubular furnace. The samples were annealed at different temperatures (260, 450, 500, or 600 °C) for 2 or 5 hours at a heating rate of 5 °C min^{-1} in a vacuum, using the vacuum pump with a suction power of 2.5 ft^3 min^{-1}.

Table 1. Experimental conditions for the synthesis of Li_3InCl_6 solid-state electrolyte.

Experiment #	Ball-milling duration (hr)	Annealing temperature (°C)	Annealing time (hr)
1	12	-	-
2	24	600	5
3	24	500	5
4	24	450	5
5	12	450	5
6	12	260	2

 doi:10.20944/preprints202311.1860.v1

2.2. Materials Characterization

The morphology and structure of the samples were characterized by scanning electron microscopy (SEM) by using the Thermo Scientific Helios 5CX) equipped with an EDX analyzer. In-situ XRD analysis at different temperatures was performed by using the EMPYREAN X-ray diffractometer from Malvern PANalytical, Co Kα λ = λ = 1.78899 Å) with a hot stage. In-situ/operand X-ray photoelectron spectroscopy was acquired from Thermo Fisher Scientific using Nexsa G2 surface analysis system with a DualBeam charge compensation system for precise analysis of the Li_3InCl_6 with negligible electronic conductivity [19].

The water absorption behavior of Li_3InCl_6 was evaluated by using thermogravimetric analysis (TGA) with scanning calorimetry. The samples (7.06 mg) were weighed in the argon glove box and transferred in a sealed container to the (SDT Q600 V20.9 Build 20). The measurements were performed under argon gas flow (100 mL min^{-1}) within the temperature range of 25 to 600 °C at a 5 °C min^{-1} scan rate.

2.3. Electrochemical Characterization

The ionic conductivity of Li_3InCl_6 powder was measured by the Solartron 1260 analyzer in the frequency range from 0.3 MHz to 1.0 Hz in a temperature range of 25 to 100 °C using an environmental chamber. For each EIS measurement, 100 mg of powder was placed within a 12 mm diameter PEEK split cell from MSE supplies equipped with two stainless-steel electrodes, a pressure jig, and a load sensor.

The solid-state electrolyte disks from the optimized Li_3InCl_6 powder (Table 1, sample 6) were produced by applying different compression forces specifically 216, 260, and 286 MPa. The ionic conductivity was determined using the following equation, σ = L/RS, where L - post-palletization thickness (cm), S- pellet area (cm^2), and R- resistance (Ω). The activation energy (E_a) was derived from the corresponding Arrhenius plots.

3. Results and discussion

3.1. Structural and thermal analysis

The X-ray diffraction (XRD) patterns of the ball-milled and annealed Li_3InCl_6 samples (Table 1) reveal varying crystallinity based on the annealing temperatures (Figure 1a). Without heat treatment, the sample ball-milled for 12 hr exhibits broad peaks indicating its low crystallinity. In contrast, all the samples heat-treated in the temperature range of 260-600 °C reveal sharp peaks and high crystallinity [15]. At lower annealing temperatures (260-450 °C), the XRD spectra match the monoclinic Li_3InCl_6 crystal structure belonging to the C2/m space group (ICCD No. 04-009-9027). However, at higher temperatures (500 and 600 °C), certain characteristic peaks of Li_3InCl_6 at approximately 2θ= 21° and 25° were absent. Particularly, the XRD pattern of the Li_3InCl_6 sample annealed at 600°C revealed the presence of an impurity phase, specifically InOCl (2θ= 12.5 °) [20]. In addition, a weak unknown peak (2θ= 15.2 °) was observed at 500 °C, which diminished as the annealing temperature decreased to 260 °C.

Furthermore, the XRD data for Li_3InCl_6 samples indicate that high-purity Li_3InCl_6 solid electrolyte can be produced with short ball-milling times (12 hr) and low annealing temperatures (260 °C). In comparison to previous reports requiring 24 hr of ball milling [15], the sample annealed at 260 °C for 2 hr and ball-milled for 12 hr (Table 1, Sample 6) are selected as the most promising candidate for further electrochemical studies, representing an optimized Li_3InCl_6.

Preprints (www.preprints.org) | NOT PEER-REVIEWED | Posted: 29 November 2023 doi:10.20944/preprints202311.1860.v1

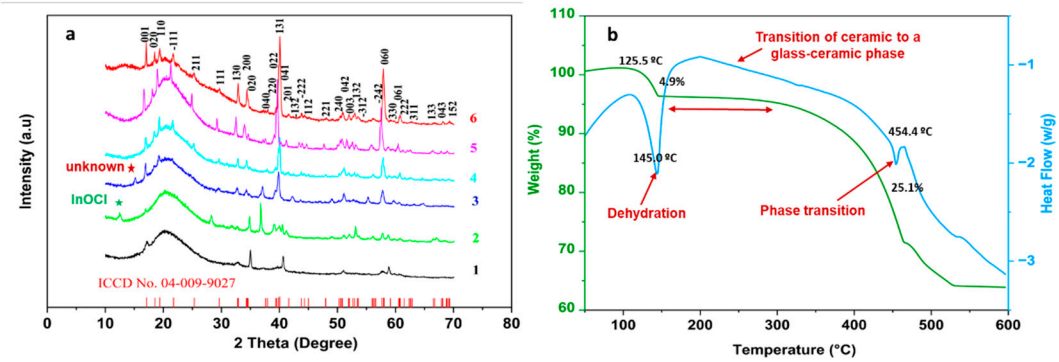

Figure 1. X-ray diffraction patterns of the ball milled and annealed Li_3InCl_6 samples, alongside the standard pattern of reported Li_3InCl_6 (ICSD No. 04-009-9027) **(a)**; Data from the TGA analysis with scanning calorimetry for the optimized Li_3InCl_6 **(b)**.

An important property of many solid-state electrolytes and, specifically, indium halides is moisture sensitivity [17]. The Li_3InCl_6 sample demonstrates moisture sensitivity, which is observed through controlled exposure to ambient air, leading to the formation of $Li_3InCl_6{\cdot}2H_2O$ [21]. Figure 1b illustrates semi-quantitative TGA/DSC data for the optimized Li_3InCl_6. The weight loss of the Li_3InCl_6 sample at 145.0 °C is 4.91%, signifying the removal of the water molecules from the Li_3InCl_6 surface and producing the corresponding endothermic effect. The second effect in the temperature range of 145 to 280 °C reveals that the mass of the Li_3InCl_6 sample remains constant. However, the endothermic effect is observed in this temperature range that could be assigned to partial and gradual transformation from ceramic to a glass-ceramic phase and evolution of chlorine from the sample, as shown in the following XPS results (Figure 5). At 454.4 °C, the third endothermic effect is observed which could be explained by further chlorine loss and phase transition. This observation provides essential insights into the material's dynamic behavior under thermal conditions.

3.2. Morphological analysis

Material morphology is vital for shaping properties and influencing material properties. Glass-ceramic solid electrolytes, with their specific morphology, show promise for solid-state electrolytes, offering enhanced ion conductivity and mechanical durability even at high temperatures [22].

Based on the results of the comparative study, the morphology of the most promising Li_3InCl_6 material was studied at different magnifications (Figure 2a–c). The Li_3InCl_6 particles exhibit characteristic agglomerate morphology consisting of smaller particles of irregular shape. Their glass-ceramic nature and particle size distribution range from 200 nm to 500 nm offer greater flexibility to tolerate the volume expansion during charge-discharge processes, lower porosity after applying compression force, and better interfacial contact, for example, with cathode nanoparticles. The elemental analysis of Li_3InCl_6 nanostructures performed by EDS revealed the Li_3InCl_6 chemical composition and uniform distribution of In and Cl with the atomic ratio of In (At. %): Cl (At. %) =1: 5.9 that matches the atomic ratio of these elements in Li_3InCl_6 (Figure 2c,d).

Preprints (www.preprints.org) | NOT PEER-REVIEWED | Posted: 29 November 2023 doi:10.20944/preprints202311.1860.v1

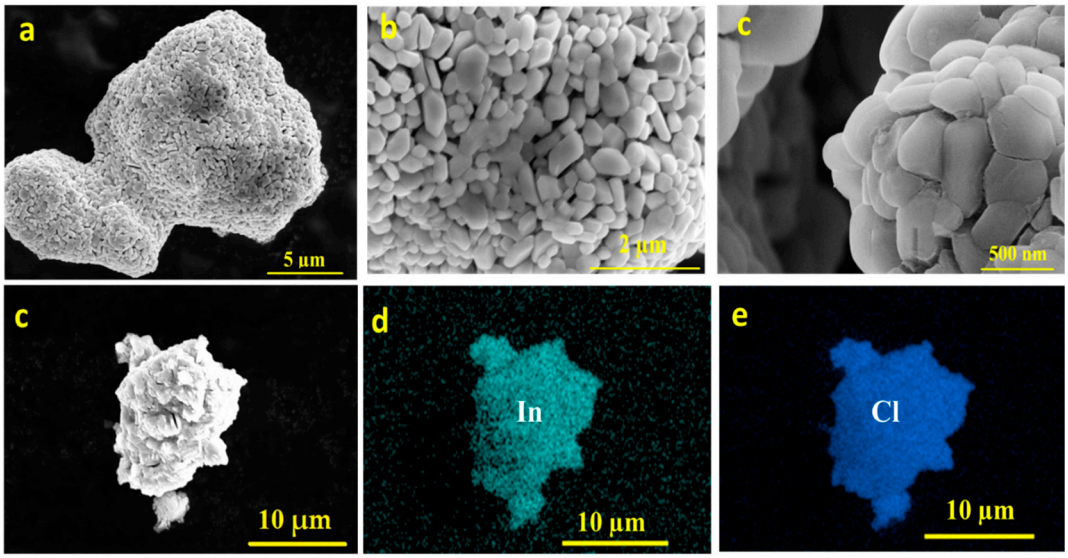

Figure 2. SEM images of the optimized Li_3InCl_6 electrolyte at different magnifications **(a-c)**; back-scattered image **(c)**; and EDS X-ray maps of indium and chloride (**d-e**).

3.3. Electrochemical performance evaluation

The ionic conductivity of the optimized Li_3InCl_6 sample was evaluated, by investigating the impact of compression force applied to the synthesized powder and varying temperatures. The Nyquist plots (Figure 3a–c) depict sample behavior under pressure ranging from 216 to 286 MPa and temperatures changing from 25 °C to 100°C for stainless steel blocking electrodes. The calculated ionic conductivities are represented by Arrhenius plots (Figure 3d–f). Notably, the sample's conductivity at room temperature decreased from 105 Ω (at 216 MPa) to 45 Ω (at 286 MPa), which translated into ionic conductivities of 0.42 mS/cm and 0.98 mS/cm, respectively. This data matches the previously published results for Li_3InCl_6 synthesized from water solutions [23].

The activation energy within the temperature range of 25-70 °C for pressures of 216, 260, and 286 MPa is 0.135, 0.116, and 0.111 eV, respectively. This fluctuation is attributed to pressure-induced modification in grain-to-grain contacts. As depicted in Figures 3d–f, Arrhenius plots consist of two fitting lines from 25 to 60 °C and 70 to 100 °C. As the temperature increases, the slope of the Arrhenius plot becomes obviously steeper above 70 °C, indicating a higher diffusion activation energy. This result could be explained by the phase transformation of the monoclinic structure to the other crystal structure at higher temperatures leading to a significant conductivity increase at and above 70 °C. In the past, similar observations were reported, for example for chlorine-based electrolytes that demonstrated orthorhombic to tetragonal/cubic phase transformations [24]. Another possible explanation for the observed increase in lithium-ion conductivity can be attributed to the decrease of the interfacial barrier at the solid electrolyte interface (SEI) at elevated temperatures [24]. These assumptions were further confirmed by applying in-situ XRD and XPS analysis.

SEM images of pellet surfaces were obtained under different pressures (Figure 4a–c). At a lower compression force of 216 MPa, the surface of the pellet is less uniform and shows more voids within the structure, yielding lower conductivity. Conversely, higher compression results in higher ionic conductivity due to increased material density and more uniform morphology, fostering increased contact between grains [25].

Preprints (www.preprints.org) | NOT PEER-REVIEWED | Posted: 29 November 2023 doi:10.20944/preprints202311.1860.v1

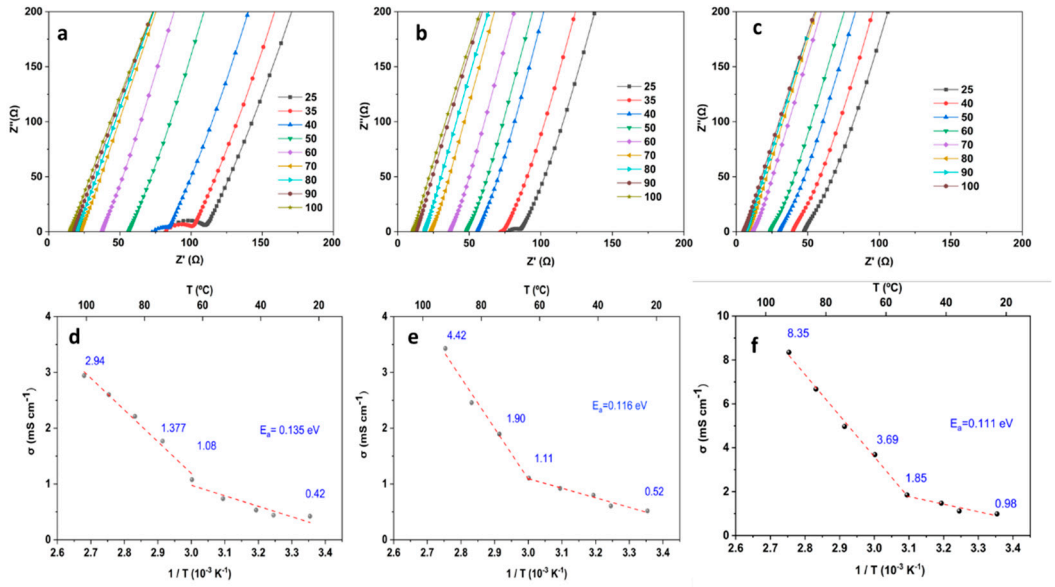

Figure 3. EIS spectra of Li_3InCl_6 electrolyte at different compression in the temperature range **(a-c)**. The corresponding Arrhenius plots for the Li_3InCl_6 solid-state electrolyte in the temperature range with different pressures demonstrate a visible phase transition at 70 °C **(d-f)**. Note: a, d results produced at 216 MPa; b, e at 260 MPa; and c, f at 286 MPa.

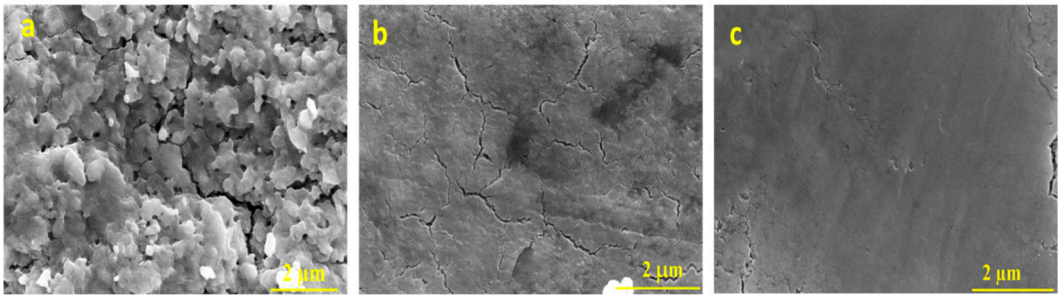

Figure 4. SEM images of the pellet surface under different compression forces of 216 MPa **(a)**; 260 MPa **(b)**; and 286 MPa **(c)**.

3.4. In-situ-XRD and XPS analysis

In-situ XRD analysis for the optimized Li_3InCl_6 electrolyte was performed by using a controlled heating method in the temperature from 25 °C to 280 °C (Figure 5a–d). Notably, visible changes in peaks are observed indicating a shift in the positions of the peaks at 2θ = 32.7.8°, 34.3°, 51.2°, 57.7°, and 59.6°, moving towards lower values within the temperature range of 70 °C to 280 °C. Interestingly, a new shoulder peak emerges at 2θ = 39.3°at 70 °C, indicating the formation of a new crystal structure. Moreover, the peaks at 2θ = 37.1°, 42.2°, and 55.1° exhibit higher intensities during this temperature change (Figure 5c,d). Interestingly, as the temperature surpasses 200 °C, these peaks gradually diminish, implying an ongoing transformative process.

Preprints (www.preprints.org) | NOT PEER-REVIEWED | Posted: 29 November 2023 doi:10.20944/preprints202311.1860.v1

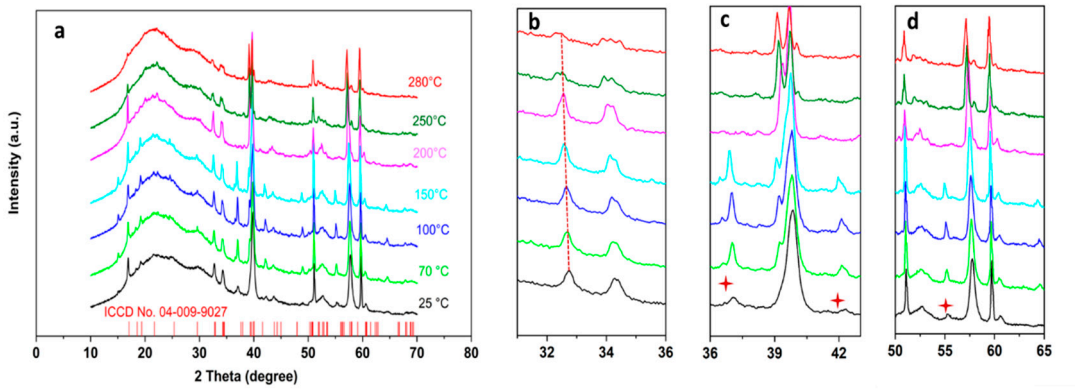

Figure 5. In-situ X-ray diffraction patterns of the optimized Li_3InCl_6 electrolyte in the temperature range of 25 -280 °C.

Though important for understanding phase transitions happening while increasing the temperature, in-situ XRD doesn't provide information about the chemical composition. This information was obtained by using in-situ/operando XPS. Figure 6a displays the binding energies corresponding to the constituent elements (O1s, In3d, Cl2p, Li1s) at different temperatures. Based on the chemical surface analysis of the Li_3InCl_6 powder (Figure 6b) the atomic percentage of these elements (O, In, Cl, Li) during the heating is changing. The O1 intensity gradually decreases up to 120°C, suggesting a potential reduction in surface oxygen concentration. However, it increases post-120°C. The In3d peak consistently decreases from 25 °C to 200 °C, followed by a slight increase up to 280 °C, implying changes in indium's chemical state or bonding environment, related to alterations in its oxidation state or bonding configuration. The Cl2p intensity decreases from room temperature to 280 °C, indicating changes in the chemical state or bonding environment of chlorine. Meanwhile, the Li1s intensity increases from 25 °C to 280 °C, with a slight upturn after 200 °C. This trend suggests alterations in the chemical state or bonding environment of lithium, potentially reflecting changes in lithium-related species.

A notable increase in ionic conductivity at temperatures above 70 °C may be associated with changes in the material's structure or phase transformation. Specifically, variations in the In3d and Li1S peaks may indicate modifications in the indium and lithium bonding environment. Phase transformations often involve alterations in the arrangement of atoms and bonding configurations, impacting the material's properties. The XPS data reveals shifts or changes in intensity, particularly in Cl2p and In3d, suggesting changes in the surface chemistry and bonding environments of chlorine and indium. Such changes could influence the material's conductivity by affecting the movement of ions, contributing to enhanced ionic conductivity.

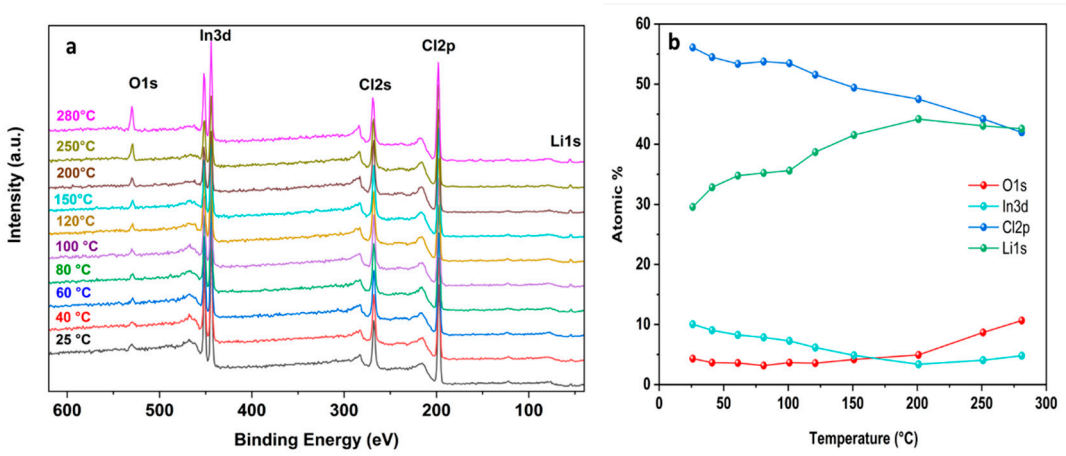

Figure 6. In-situ XPS of Li_3InCl_6 at different temperatures **(a)**; Atomic percentages of elements with changing temperatures **(b).**

4. Conclusion

In summary, a comprehensive understanding of the ionic conductivity in the halide SSE of Li_3InCl_6 across a broad temperature range was revealed for the first time. This was achieved through the integration of ex-situ EIS, TGA/DSC, and in-situ characterization methods, such as in-situ X-ray and XPS analysis. Compared to other publications, the optimized material with high ionic conductivity of about 1.0 $mS \cdot cm^{-1}$ was synthesized at a much lower temperature (260 ^oC) and shorter ball-milling time, while applying a compression force of 286 MPa.

Our findings highlight the enhancement in Li_3InCl_6 ionic conductivity at elevated temperatures that can be ascribed to the changes in the material's composition, particularly evident in the altered chemical states and bonding environments of indium, chlorine, and lithium. After the surface-bound water is lost, the mass of Li_3InCl_6 remains constant up to 280 ^oC. However, a negative heat flow is observed that could be assigned to ceramic/ glass transformations and changes in chemical composition. In-situ XRD and XPS analyses confirm the assumptions regarding structural and chemical changes during temperature variations. The emergence of new peaks in XRD patterns and shifts in XPS binding energies indicate phase transformations and alterations in the chemical states or bonding environments of constituent elements. Notably, changes in indium and lithium bonding environments may contribute to the observed increase in ionic conductivity above 70 °C and phase transformation at 454.4 ^oC as confirmed by the TGA analysis. Consequently, the application of this electrolyte in industrial contexts holds both feasibility and substantial promise.

Author Contributions: Conceptualization, F.B. and A.S.; methodology, F.B.; software, F.B.; validation, F.B., and A.S.; formal analysis, F.B.; investigation, F.B., and A.S; resources, F.B. and A.S; data acquisition, F.B., C.R., P.M., and K.L.; writing—original draft preparation, F.B.; writing—review and editing, F.B. and A.S.; supervision, A.S.; project administration, F.B., and A.S; funding acquisition, A.S. All authors have read and agreed to the published version of the manuscript.

Funding: The authors acknowledge financial support from the NSF IUCRC program for supporting the ''Center for Solid-state Electric Power Storage (CEPS)'' and the South Dakota "Governor's Research Center for Electrochemical Energy Storage''.

Data Availability Statement: Data Availability Statement: Data available on request. The data presented in this study are available on request from the corresponding author.

Acknowledgments: The authors gratefully acknowledge the administrative and technical support from faculty and students at the South Dakota School of Mines and Technology.

Conflicts of Interest: The authors declare no conflict of interest.

References

1. Wang, S.; Wu, Y.; Ma, T.; Chen, L.; Li, H.; Wu, F., Thermal stability between sulfide solid electrolytes and oxide cathode. ACS nano **2022**, 16 (10), 16158-16176. https://doi.org/10.1021/acsnano.2c04905
2. Luo, X.; Cai, D.; Wang, X.; Xia, X.; Gu, C.; Tu, J., A novel ethanol-mediated synthesis of superionic halide electrolytes for high-voltage all-solid-state lithium–metal batteries. *ACS Appl. Mater. Interfaces* **2022**, *14 (26)*, 29844-29855. https://doi.org/10.1021/acsami.2c06216
3. Peng, J.; Wu, D.; Lu, P.; Wang, Z.; Du, Y.; Wu, Y.; Wu, Y.; Yan, W.; Wang, J.; Li, H., High-safety, wide-temperature-range, low-external-pressure and dendrite-free lithium battery with sulfide solid electrolyte. *Energy Stor.* Mater. **2023**, *54*, 430-439. https://doi.org/10.1016/j.ensm.2022.10.057
4. Asano, T.; Sakai, A.; Ouchi, S.; Sakaida, M.; Miyazaki, A.; Hasegawa, S., Solid halide electrolytes with high lithium-ion conductivity for application in 4 V class bulk-type all-solid-state batteries. *Adv. Mater.* **2018**, *30 (44)*, 1803075. https://doi.org/10.1002/adma.201803075
5. Chen, R.; Li, Q.; Yu, X.; Chen, L.; Li, H., Approaching practically accessible solid-state batteries: stability issues related to solid electrolytes and interfaces. *Chem. Rev.* **2019**, *120 (14)*, 6820-6877. https://doi.org/10.1021/acs.chemrev.9b00268

6. Trahey, L.; Brushett, F. R.; Balsara, N. P.; Ceder, G.; Cheng, L.; Chiang, Y.-M.; Hahn, N. T.; Ingram, B. J.; Minteer, S. D.; Moore, J. S., Energy storage emerging: A perspective from the Joint Center for Energy Storage Research. *Proc. Natl. Acad. Sci.* **2020**, *117 (23)*, 12550-12557. https://doi.org/10.1073/pnas.1821672117
7. Famprikis, T.; Canepa, P.; Dawson, J. A.; Islam, M. S.; Masquelier, C., Fundamentals of inorganic solid-state electrolytes for batteries. *Nat. Mater.***2019**, *18 (12)*, 1278-1291. https://doi.org/10.1038/s41563-019-0431-3
8. Zhu, Y.; Mo, Y., Materials design principles for air-stable lithium/sodium solid electrolytes. *Angew. Chem., Int. Ed.* **2020**, *59 (40)*, 17472-17476. https://doi.org/10.1002/anie.202007621
9. Xu, R.; Wang, X.; Zhang, S.; Xia, Y.; Xia, X.; Wu, J.; Tu, J., Rational coating of Li7P3S11 solid electrolyte on MoS2 electrode for all-solid-state lithium-ion batteries. *J. Power Sources.* **2018**, *374*, 107-112. https://doi.org/10.1016/j.jpowsour.2017.10.093
10. Auvergniot, J.; Cassel, A.; Ledeuil, J.-B.; Viallet, V.; Seznec, V.; Dedryvère, R., Interface stability of argyrodite Li6PS5Cl toward LiCoO2, LiNi1/3Co1/3Mn1/3O2, and LiMn2O4 in bulk all-solid-state batteries. *Chem. Mater.* **2017**, 29 (9), 3883-3890. https://doi.org/10.1021/acs.chemmater.6b04990
11. Wang, D.; Sun, Q.; Luo, J.; Liang, J.; Sun, Y.; Li, R.; Adair, K.; Zhang, L.; Yang, R.; Lu, S., Mitigating the interfacial degradation in cathodes for high-performance oxide-based solid-state lithium batteries. *ACS Appl. Mater. Interfaces* **2019**, *11 (5)*, 4954-4961. https://doi.org/10.1021/acsami.8b17881
12. Lu, P.; Liu, L.; Wang, S.; Xu, J.; Peng, J.; Yan, W.; Wang, Q.; Li, H.; Chen, L.; Wu, F., Superior all-solid-state batteries enabled by a gas-phase-synthesized sulfide electrolyte with ultrahigh moisture stability and ionic conductivity. *Adv. Mater.* **2021**, *33 (32)*, 2100921. https://doi.org/10.1002/adma.202100921
13. Thangadurai, V.; Narayanan, S.; Pinzaru, D., Garnet-type solid-state fast Li-ion conductors for Li batteries: critical review. *Chem. Soc. Rev.* **2014**, *43 (13)*, 4714-4727. https://doi.org/10.1039/C4CS00020J
14. Sakuma, M.; Suzuki, K.; Hirayama, M.; Kanno, R., Reactions at the electrode/electrolyte interface of all-solid-state lithium batteries incorporating Li–M (M= Sn, Si) alloy electrodes and sulfide-based solid electrolytes. *Solid State Ion.* **2016**, *285*, 101-105. https://doi.org/10.1016/j.ssi.2015.07.010
15. Li, X.; Liang, J.; Luo, J.; Banis, M. N.; Wang, C.; Li, W.; Deng, S.; Yu, C.; Zhao, F.; Hu, Y., Air-stable Li 3 InCl 6 electrolyte
16. with high voltage compatibility for all-solid-state batteries. Energy Environ. Sci. 2019, 12 (9), 2665-2671 https://doi.org/10.1039/C9EE02311A
17. Zhou, L.; Zuo, T.-T.; Kwok, C. Y.; Kim, S. Y.; Assoud, A.; Zhang, Q.; Janek, J.; Nazar, L. F., High areal capacity, long cycle life 4 V ceramic all-solid-state Li-ion batteries enabled by chloride solid electrolytes. *Nat. Energy* **2022**, 7 (1), 83-93. https://doi.org/10.1038/s41560-021-00952-0
18. Li, X.; Liang, J.; Chen, N.; Luo, J.; Adair, K. R.; Wang, C.; Banis, M. N.; Sham, T. K.; Zhang, L.; Zhao, S., Water-mediated synthesis of a superionic halide solid electrolyte. Angew. Chem 2019, 131 (46), 16579-16584. https://doi.org/10.1002/ange.201909805
19. Li, W.; Liang, J.; Li, M.; Adair, K. R.; Li, X.; Hu, Y.; Xiao, Q.; Feng, R.; Li, R.; Zhang, L., Unraveling the origin of moisture stability of halide solid-state electrolytes by in situ and operando synchrotron X-ray analytical techniques. *Chem. Mater.* **2020**, *32 (16)*, 7019-7027. https://doi.org/10.1021/acs.chemmater.0c02419
20. Deng, S.; Jiang, M.; Chen, N.; Li, W.; Zheng, M.; Chen, W.; Li, R.; Huang, H.; Wang, J.; Singh, C. V., Regulating Electronic Conductivity at Cathode Interface for Low-Temperature Halide-Based All-Solid-State Batteries. *Adv. Funct. Mater.* **2022**, 32 (45), 2205594. https://doi.org/10.1002/adfm.202205594
21. Wang, K.; Ye, Q.; Zhang, J.; Huang, H.; Gan, Y.; He, X.; Zhang, W., Halide electrolyte Li3InCl6-based all-solid-state lithium batteries with slurry-coated LiNi0. 8Co0. 1Mn0. 1O2 composite cathode: effect of binders. *Front. Mater* **2021**, *8*, 727617. https://doi.org/10.3389/fmats.2021.727617
22. Wang, S.; Xu, X.; Cui, C.; Zeng, C.; Liang, J.; Fu, J.; Zhang, R.; Zhai, T.; Li, H., Air sensitivity and degradation evolution of halide solid-state electrolytes upon exposure. *Adv. Funct. Mater.* **2022**, 32 (7), 2108805. https://doi.org/10.1002/adfm.202108805
23. Gandi, S.; Chidambara Swamy Vaddadi, V. S.; Sripada Panda, S. S.; Goona, N. K.; Parne, S. R.; Lakavat, M.; Bhaumik, A., Recent progress in the development of glass and glass-ceramic cathode/solid electrolyte materials for next-generation high capacity all-solid-state sodium-ion batteries: A review. *J. Power Sources* 2022, 521, 230930. https://doi.org/10.1016/j.jpowsour.2021.230930
24. Sacci, R. L.; Bennett, T. H.; Drews, A. R.; Anandan, V.; Kirkham, M. J.; Daemen, L. L.; Nanda, J., Phase evolution during lithium–indium halide superionic conductor dehydration. J. Mater. Chem. A **2021**, 9 (2), 990-996. https://doi.org/10.1039/D0TA10012A

25. Song, A. Y.; Xiao, Y.; Turcheniuk, K.; Upadhya, P.; Ramanujapuram, A.; Benson, J.; Magasinski, A.; Olguin, M.; Meda, L.; Borodin, O., Protons enhance conductivities in lithium halide hydroxide/lithium oxyhalide solid electrolytes by forming rotating hydroxy groups. *Adv. Energy Mater* **2018**, *8 (3)*, 1700971. https://doi.org/10.1002/aenm.201700971
26. Molaiyan, P.; Mailhiot, S. E.; Voges, K.; Kantola, A. M.; Hu, T.; Michalowski, P.; Kwade, A.; Telkki, V.-V.; Lassi, U., Investigation of the structure and ionic conductivity of a Li3InCl6 modified by dry room annealing for solid-state Li-ion battery applications. *Mater. Des.* **2023**, *227*, 111690. https://doi.org/10.1016/j.matdes.2023.111690